NANO · MICRO small
www.small-journal.com

Tailoring Writability and Performance of Star Block Copolypeptides Hydrogels through Side-Chain Design

Ronnie V. Garcia, Elizabeth A. Murphy, Nairiti J. Sinha, Yoichi Okayama, Juan Manuel Urueña, Matthew E. Helgeson, Christopher M. Bates, Craig J. Hawker, Robert D. Murphy, and Javier Read de Alaniz**

Shear-recoverable hydrogels based on block copolypeptides with rapid self-recovery hold potential in extrudable and injectable 3D-printing applications. In this work, a series of 3-arm star-shaped block copolypeptides composed of an inner hydrophilic poly(L-glutamate) domain and an outer β-sheet forming domain is synthesized with varying side chains and block lengths. By changing the β-sheet forming domains, hydrogels with diverse microstructures and mechanical properties are prepared and structure–function relationships are determined using scattering and rheological techniques. Differences in the properties of these materials are amplified during direct-ink writing with a strong correlation observed between printability and material chemistry. Significantly, it is observed that non-canonical β-sheet blocks based on phenyl glycine form more stable networks with superior mechanical properties and writability compared to widely used natural amino acid counterparts. The versatile design available through block copolypeptide materials provides a robust platform to access tunable material properties based solely on molecular design. These systems can be exploited in extrusion-based applications such as 3D-printing without the need for additives.

1. Introduction

Additive manufacturing or 3D-printing of hydrogels combines complex geometrical control with functional material selection for diverse applications in electronics,[1] structural materials,[2] and biomedicine.[3] Consequently, 3D-printed hydrogels are an emerging area of focus with advantages including tunability, high water content, and potential biocompatibility.[4–6] For light-based 3D-printing such as stereolithography and digital-light processing, hydrogels must be formulated to have low viscosities and undergo rapid photocrosslinking.[7–9] In contrast, extrusion techniques like direct-ink writing (DIW) rely on formulations with a shear-recoverable yield stress to achieve high-fidelity shapes.[10,11] Traditionally, 3D-printable hydrogels are based on natural biopolymers such as gelatin or alginate as the key biopolymer building block.[12] However, these materials suffer from several limitations including batch-to-batch variation and an inability to systematically tune their molecular structure.[13] Due to these constraints, the printability of natural biopolymers can only be modulated by concentration,[14] additives,[15] or multi-component blends.[16,17] For example, native alginate cannot be used directly in DIW; calcium ions or clay particles are required to achieve the necessary shear-thinning properties.[13] Although synthetic material systems such as poloxamers are chemically tunable, there are still drawbacks. For example, the sol–gel temperature of poloxamer 407 is sensitive to a multitude of factors. Moreover, poloxamers lack inherent biodegradability that is desirable for biological applications.[18] To further expand this area of research and diversify the palette

R. V. Garcia, E. A. Murphy, N. J. Sinha, C. M. Bates, C. J. Hawker, J. Read de Alaniz
Department of Chemistry & Biochemistry
University of California
Santa Barbara, Santa Barbara, CA 93106, USA
E-mail: hawker@mrl.ucsb.edu; javier@chem.ucsb.edu

R. V. Garcia, E. A. Murphy, N. J. Sinha, Y. Okayama, M. E. Helgeson, C. M. Bates, C. J. Hawker, R. D. Murphy, J. Read de Alaniz
Materials Research Laboratory
University of California
Santa Barbara, Santa Barbara, CA 93106, USA

R. V. Garcia, J. M. Urueña, M. E. Helgeson, C. M. Bates, C. J. Hawker, J. Read de Alaniz
BioPACIFIC Materials Innovation Platform
University of California
Santa Barbara, Santa Barbara, CA 93106, USA

N. J. Sinha, M. E. Helgeson, C. M. Bates
Department of Chemical Engineering
University of California
Santa Barbara, Santa Barbara, CA 93106, USA

C. M. Bates, C. J. Hawker
Materials Department
University of California
Santa Barbara, Santa Barbara, CA 93106, USA

The ORCID identification number(s) for the author(s) of this article can be found under https://doi.org/10.1002/smll.202302794

DOI: 10.1002/smll.202302794

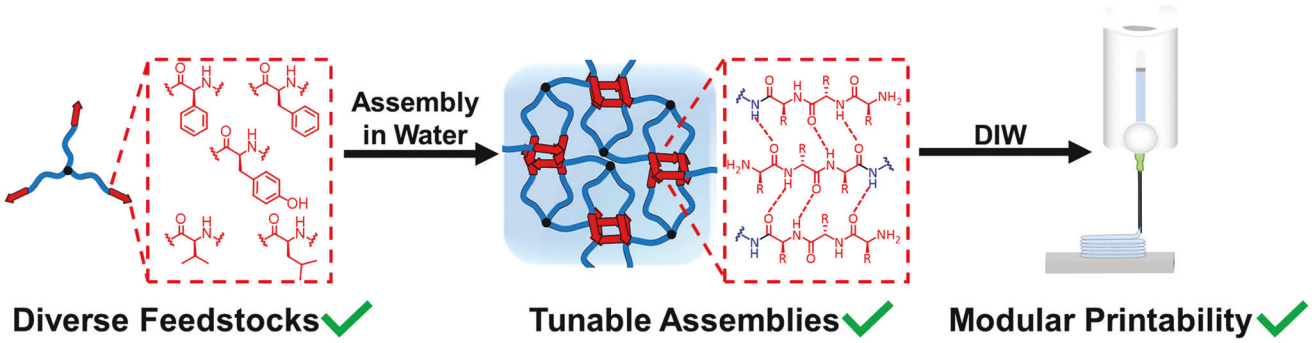

Figure 1. Modular design of 3-arm block copolypeptide enables tunable microstructure and properties based on amino acid selection.

of 3D-printable hydrogels, there is a need to explore shear-recoverable materials that can be synthetically tuned without sacrificing the inherent benefits of biopolymers, ranging from degradability to sustainable sourcing and biocompatibility.

Block copolypeptides with controllable composition, molecular weight, and topology are attractive alternatives to traditional biopolymers for DIW 3D-printing application. An enabling synthetic technique to access these materials involves the ring-opening polymerization (ROP) of *N*-carboxyanhydrides (NCAs) leading to scalable block copolypeptides with well-defined molecular weight and architectures.[19] A variety of non-covalent bonding interactions, such as hydrogen bonding and π–π stacking, can be further integrated into these materials by engineering the peptide backbone and side chain to create hierarchical structures. The intrinsic chirality of the peptide backbone also allows for adoption of distinct secondary structures such as α-helices, β-sheet, and hairpin motifs to further influence material properties.[11,20–27] Through rational design, copolypeptide inner blocks that contain electrostatics promote high water absorption, while careful choice of the outer block(s) yields strongly associating β-sheet domains that lead to robust hydrogel networks stabilized by reversible physical crosslinks.[28] These properties have high utility for extrusion and rapid recovery, eliminating the need for rheological additives.[29] Based on a similar principle, Hartgerink and co-workers have also developed nanofibrous hydrogel comprised of multidomain peptides with good viscoelastic properties for DIW.[30] Designer block copolypeptides have therefore found use as injectable carriers, tissue engineering scaffolds, antimicrobial materials, and more recently 3D-printable bioinks.[31–37]

Recently, our group demonstrated the synthetic versatility of block copolypeptides and their applicability to the development of bioinks that can be chemically crosslinked with visible light.[38] This strategy generates well-defined, viable biocomposites with *Escherichia coli*, controlling the behavior of embedded bacteria by modulating mechanical properties of the host block copolypeptide hydrogel through a functional-group change in associating domains. Further understanding structure–function relationships in these physically crosslinked junctions is critical to extend the generality of this approach and tune performance by varying block chemistry, concentration, and architecture.[39–42] In particular, the effect of side-chain amino acids has not been studied extensively and is hypothesized to dictate associating-domain formation and related hydrogel properties such as rheological regimes, which are crucial for extrusion-based applications.

Here, we investigate the synthesis of five different, 3-arm, block copolypeptide stars which have a fixed-length inner domain of polyglutamate but differ in the nature of the side chains attached to the outer peptide block. The impact of these changes on hydrogel microstructure, properties, and printability are studied (**Figure 1**). While block copolypeptides containing cationic polylysine inner blocks have been widely studied, anionic polyglutamates are of interest due to the carboxyl groups serving as sites for cation-chelating and post-polymerization modification.[38] Amino acids incorporated into the outer blocks were selected based on their propensity to form hydrophobic and π–π interactions in order to correlate chain structure with β-sheet network strength. Specifically, 3-arm block copolypeptides (3-CP) with the same polyglutamic acid core and outer blocks containing valine (3-CP-V), leucine (3-CP-L), tyrosine (3-CP-T), phenyl glycine (3-CP-PG), and phenylalanine (3-CP-PA) were investigated. Phenyl-glycine–containing outer blocks (3-CP-PG) were also synthesized to showcase the use of a non-natural amino acid to control interactions and assembly of these materials. Physical hydrogels readily form after dispersing in aqueous media and the underlying microstructure of these networks was elucidated using small-angle X-ray scattering (SAXS). Viscoelasticity and extrudability were evaluated using rheological characterization with representative materials 3D-printed on a commercial DIW system to showcase the ability to control 3D object and printing performance.

2. Results and Discussion

2.1. Molecular Design and Synthesis

Hydrophobic and hydrophilic amino acids were selected to investigate a wide variety of supramolecular interactions and structures by modulating β-sheet assemblies which give rise to physically crosslinked junctions. Specifically, NCA monomers based on γ-benzyl-L-glutamate (BLG), L-tyrosine (LT), L-leucine (LL), L-phenylalanine (LPA), L-phenylglycine (LPG), and L-valine (LV) were prepared using a procedure adapted from literature based on epichlorohydrin as HCl scavenger.[43] The trifunctional initiator tris(2-aminoethyl)amine (TREN) was then selected for controlled *N*-carboxyanhydride ring-opening polymerization (NCA ROP) of BLG NCA. The 3-arm architecture was chosen due to the ability of outer block domains to form 3D extended networks at lower weight percentages, enabling access to superior hydrogels compared to linear analogues.[39,44]

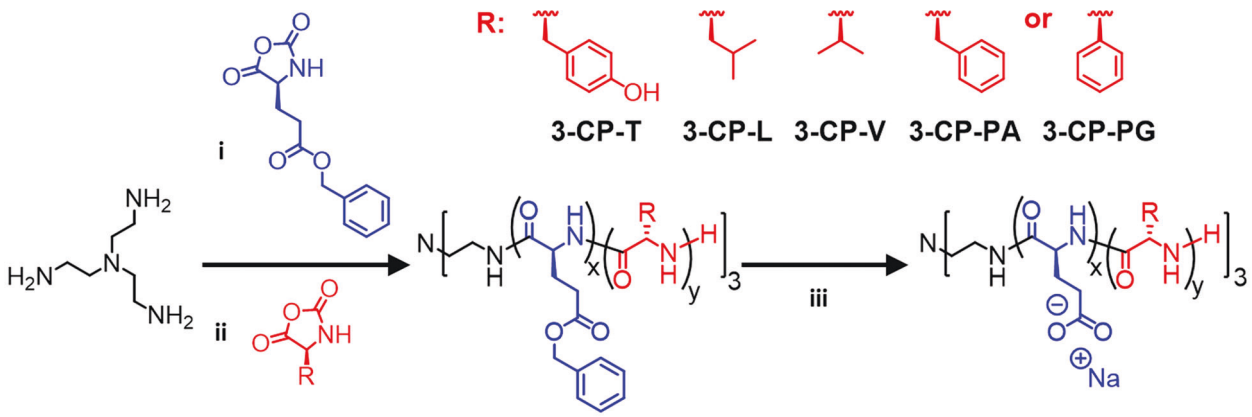

Figure 2. i) $CHCl_3$/DMF, 18 h, rt. ii) DMF (for L-tyrosine NCA) or $CHCl_3$/DMF (for other NCAs), 18 h, rt. iii) TFA/$CHCl_3$, HBr 33 wt% in AcOH, 18 h, rt; NaOH, dialysis, 3 days.

High conversions were observed with Fourier-transform infrared spectroscopy (FTIR) spectroscopy for 3-arm poly(benzyl-L-glutamate) (3-$PBLG_{80}$) with a degree of polymerization (DP) equal to ≈80 based on ^{1}H nuclear magnetic resonance (^{1}H NMR) spectroscopy.[45] The 3-$PBLG_{80}$ macroinitiator was then used to chain extend in situ with NCA's based on LT, LL, LPA, LPG, or LV, leading to β-sheet forming polymer blocks with a target DP of 45. The library of 3-arm block copolypeptides (CP) included poly(benzyl-L-glutamate-*b*-L-tyrosine) (3-$PBLG_{80}$-*b*-PLT_{33} [3-CP-T]), poly(benzyl-L-glutamate-*b*-L-valine) (3-$PBLG_{80}$-*b*-PLV_{36} [3-CP-V]), poly(benzyl-L-glutamate-*b*-L-leucine) (3-$PBLG_{80}$-*b*-PLL_{39} [3-CP-L]), poly(benzyl-L-glutamate-*b*-L-phenylalanine) (3-$PBLG_{80}$-*b*-$PLPA_{37}$ [3-CP-PA]), and poly(benzyl-L-glutamate-*b*-L-phenylglycine) (3-$PBLG_{80}$-*b*-$PLPG_{30}$ [3-CP-PG]), which were fully characterized via ^{1}H NMR spectroscopy (**Figure 2**). To understand the effect of molecular weight on hydrogel assembly, two additional block copolypeptides (3-$PBLG_{76}$-*b*-$PLPG_{16}$ [3-CP-PG-1] and 3-$PBLG_{76}$-*b*-$PLPG_{28}$ [3-CP-PG-2]) were also prepared from a common macroinitiator, 3-$PBLG_{76}$. Note that the sample nomenclature places the degree of polymerization for each block as a subscript.

The chemical structure and DP of each block copolypeptide were confirmed using ^{1}H NMR spectroscopy, with molecular weights and dispersities characterized by diffusion-ordered spectroscopy (DOSY) and size-exclusion chromatography (SEC) (Figures S7–S23, Supporting Information). It is noteworthy that high end-group retention during polymerization enabled efficient block extensions as supported by SEC and the observation of a single population by DOSY NMR for all samples. Moreover, excellent control over the ring-opening polymerization initiated by TREN was evidenced by low molar-mass dispersities ($Đ \approx 1.1$), with good agreement between experimental and targeted molecular weights. It should be noted that high molecular-weight assemblies were observed by SEC for both valine and phenyl glycine block copolypeptides, likely due to strong association of their β-sheet secondary structures in the eluent hexafluoroisopropanol (HFIP). The size of observable diblock assemblies for phenyl glycine appeared to be dependent on length (Figures S21 and S23, Supporting Information). Interestingly, DOSY NMR displays a single population due to the ability of the solvent, 15% trifluoracetic acid in deuterated chloroform ($CDCl_3$), to disrupt β-sheet formation more efficiently compared to the SEC eluent (HFIP). To afford the desired water soluble 3-arm block copolypeptides, the benzyl protecting group on the glutamate blocks was deprotected using 33 wt% hydrogen bromide (HBr) in acetic acid, followed by ionization to the sodium salt using sodium hydroxide (NaOH). Subsequent dialysis of block copolypeptides using a 10 kDa molecular weight cut off membrane was used to remove impurities and the resulting 3-arm star block copolypeptides were lyophilized and stored as dry powders for subsequent studies.

2.2. Characterization of Physical Hydrogel Self-Assembly in Water

The desired weight fraction (wt%) of 3-arm star block copolypeptides were dispersed in deionized water by mechanically mixing until a homogeneous translucent physical hydrogel is achieved. To confirm the formation of the β-sheet secondary structure at these molecular weights and dispersity of these hydrogels, FTIR in deuterated water (D_2O) showed the expected amide I bands from 1630–1690 cm^{-1} (Figure S24, Supporting Information).[46]

Since the gelation of these materials is driven by network formation of β-motif-rich junctions, SAXS was employed to gain insight into the impact of side-chain chemistry on microstructure. For subsequent studies, all physical hydrogels were compared at 40 wt% to achieve adequate contrast between water and the network topology on SAXS. The presence of negatively charged glutamate residues in the internal block domains inserts interaction peaks into the scattering signal, which precludes accurate interpretation of the data with respect to the impact of outer block characteristics (Figures S25 and S26, Supporting Information). Therefore, SAXS measurements were performed using different concentrations of sodium chloride (NaCl) in water to screen electrostatic interactions.[47] **Figure 3** shows the SAXS curves for the five amino acid types in 50 mM salt that highlight the key differences between the nanostructures of the different amino acids employed within the outer block.

In SAXS measurements, the scattering intensity $I(q)$ is a function of the magnitude of the scattering wave vector q with an approximate correspondence with a length scale $d \approx 2\pi/q$.[48] The scattering profiles of 3-arm block copolypeptide physical gels

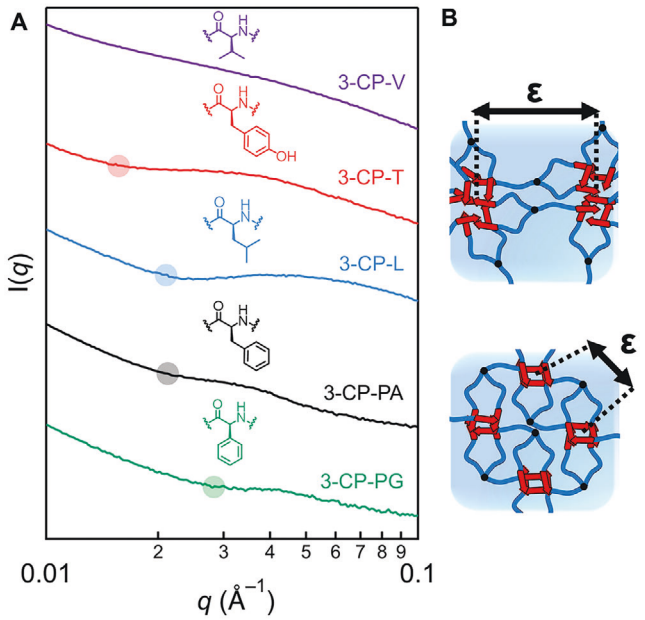

Figure 3. A) Small-angle X-ray scattering (SAXS) profiles of a 3-arm block copolypeptide library at 40 wt% in 50 mM NaCl solution with the highlighted q values corresponding to each average interdomain spacing (ε). B) Schematic depicts change in ε as aggregate sizes increase due to increase in ε-sheet strength.

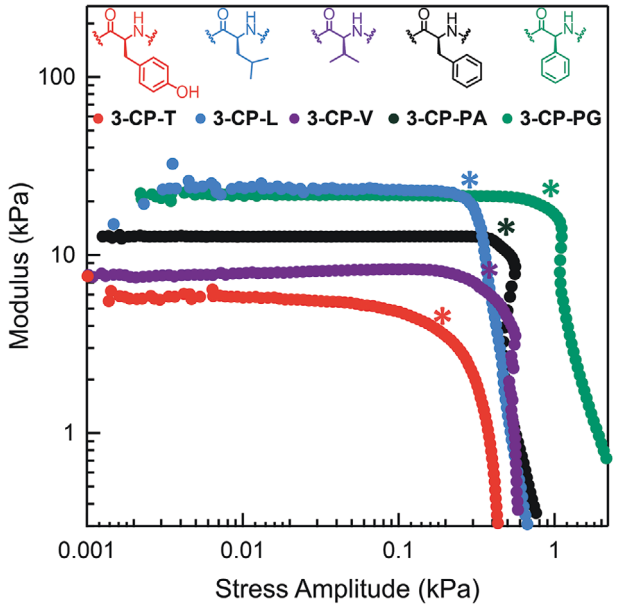

Figure 4. Storage modulus (G') of 3-arm block copolypeptide hydrogel series at 20 wt% in an oscillatory amplitude stress sweep at a constant 6.2 rad s^{-1} with yield points marked with (*).

reveal two features consistent with previous studies. The first is a broad shoulder at high q-values indicative of interdomain spacing of the β-sheet forming amino acids that comprise the physical crosslinks within the hydrogel.[48,49] The second region is a low-q increase in scattering intensity that is related to the fractal-like characteristics of the overall network structure.[50] The q-value at the transition, q^*, was used to estimate an apparent interdomain spacing, $\varepsilon = 2\pi/q^*$ within the physically-crosslinked networks. A step minimum is used to extrapolate the value of q^* for each hydrogel and is shown on the curves in Figure 3A with colored circles (see Table S1, Supporting Information, for values). Specifically for 3-CP-V, unrestricted β-sheet aggregation causes the formation of a network of aggregates from which an interdomain spacing could not be extracted.[51,52] In the remainder of the series of physical gels with fixed length of the outer block domain, 3-CP-PG exhibited the smallest ε whereas 3-CP-T exhibited the largest. This is consistent with the choice of amino acid in the outer-block, whereby we expect that changes in the degree of β-sheet aggregation can be correlated to changes in the average size and number of aggregate domains within the network, and therefore the average value of ε for materials at a fixed polypeptide concentration. Compared to the other samples, it should be noted that 3-CP-L shows a stronger helical character in the glutamate inner core, along with β-sheet assembly due to the outer leucine block (Figure S24, Supporting Information), with the interplay between these two assembly processes complicating structure–function interpretation. To further probe the impact of outer-block arm length on ε, we synthesized two different molecular weight 3-arm stars, 3-CP-PG-1 and 3-CP-PG-2, with a DP of 16 and 28, respectively for the outer block length. SAXS measurements demonstrated a slight increase in ε with longer β-sheet–forming outer blocks (Figure S26 and Table S1, Supporting Information), again consistent with the formation of larger aggregates. We therefore infer that the amino-acid selection and DP of the outer-block impacts characteristic length scales within hydrogel networks based on their proclivity to form β-sheet aggregate domains, where the trend follows 3-CP-V > 3-CP-T > 3-CP-L > 3-CP-PA > 3-CP-PG.

2.3. Tunable Viscoelasticity Based on Side-Chain Design

An advantage of this tunable material platform is an opportunity to control rheological properties via molecular design. To probe the stability and shear processing behavior of the networks, oscillatory shear measurements were conducted at different frequencies and strain amplitudes using a fixed concentration of 20 wt% copolypeptide. This concentration was chosen to minimize the use of material during optimization studies while staying above the critical concentration of the weakest hydrogelator. The strongest hydrogelators, 3-CP-PG and 3-CP-PA, can form hydrogel as low as 5 wt%, while the weakest hydrogelators such as 3-CP-L and 3-CP-T need 20 wt% to form stable homogeneous hydrogels. At low strain amplitudes in the linear viscoelastic regime, the storage modulus (G') is higher than the loss modulus (G'') at all measured frequencies, consistent with a robust physical gel (Figure S28, Supporting Information). The same is also true under low imposed stresses, indicating the hydrogels behave like stable viscoelastic solids (Figure S29, Supporting Information). The yield stress, associated with deviation from the plateau of the linear viscoelastic regime, can be attributed to chain pull out between β-sheet domains (**Figure 4**).[53] The yield point was estimated from a critical value of tan δ as indicated in Figure S30, Supporting Information, to extract the apparent yield stress. Furthermore, the pronounced flow point where tan $\delta = 1$ is related

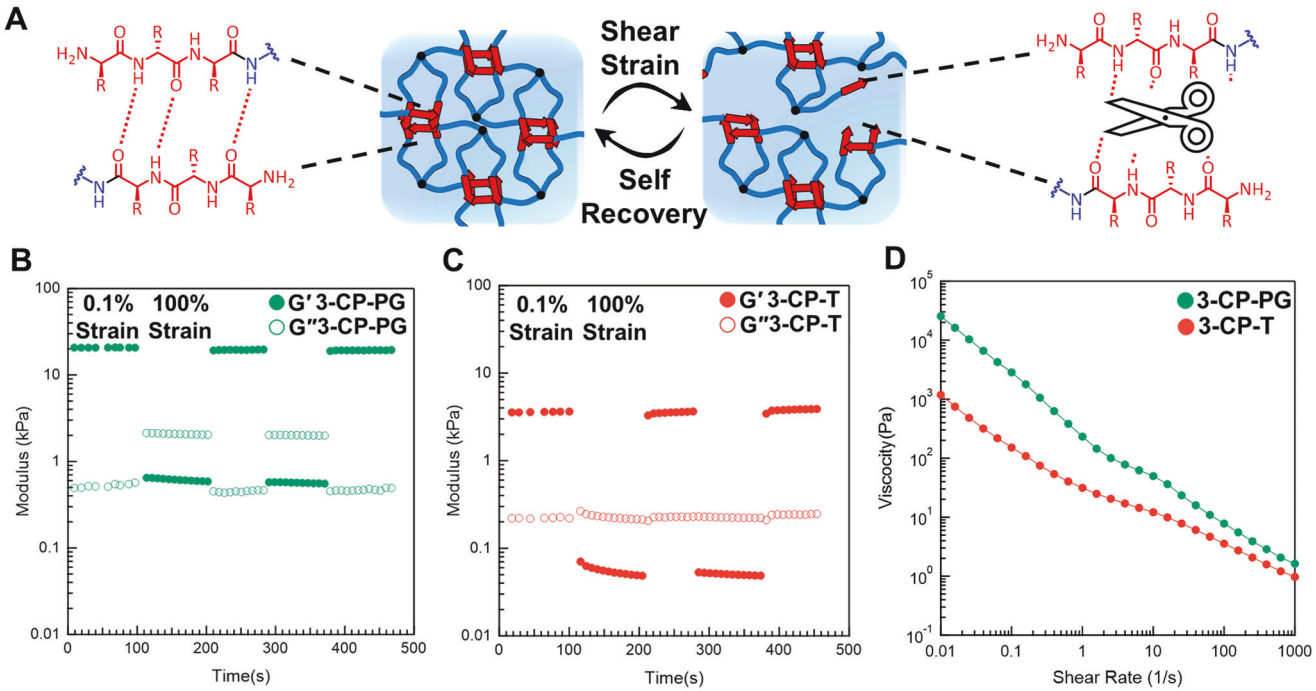

Figure 5. A) Illustration of reversible yielding behavior in copolypeptide hydrogels due to the breaking and reforming of peptide backbone H-bonding. Cyclic oscillatory strain experiments on 20 wt%. B) 3-CP-PG and C) 3-CP-T showing the network response to low (0.1%) and high (100%) strains at intervals of 100 s with a constant angular frequency of 6.2 rad s^{-1}. D) Viscosity sweep with increasing shear rate illustrating shear-thinning behavior.

to the loss of mechanical rigidity due to a sufficient number of chains between β-sheet domains no longer being connected to form the overall network (Figures S29 and S30, Supporting Information).[53,54] These two properties are critical to consider for extrusion based 3D-printing.

This system enables the creation of materials with modulus and yielding behavior influenced specifically by the side-chain amino acid chemistry with analysis under identical concentrations (Figures S29–S31, Supporting Information). For example, aryl-containing materials 3-CP-PG and 3-CP-PA exhibited a higher yield stress due to strong π–π interactions within β-sheet domains. By contrast, weaker alkyl hydrophobic interactions formed in 3-CP-L and 3-CP-V hydrogels lead to lower yield stresses. The use of 3-CP-T demonstrated that altering the polarity of the β-sheet domain by incorporating more polar phenolic side chains resulted in the weakest hydrogel network.

Phenyl glycine was selected as the lead material for subsequent studies, since its lack of flexible hydrocarbon spacer in comparison to phenyl alanine allows for increased β-sheet stability. This subtle deviation from 3-CP-PA proved to be critical as 3-CP-PG outperformed other materials, exhibiting the highest modulus and yield point. The imposed stresses associated with yielding were consisted with the hydrogel interdomain spacing, where hydrogels having smaller average interdomain spacing ε (i.e., higher density of physical crosslinking centers) exhibit higher elastic modulus and yield stress. Overall, the combined structural and rheological measurements reveal the side chain chemistry to be an important and synthetically tunable parameter that controls β-sheet interactions, physical crosslinking structure, and the corresponding rheological properties of these hydrogels.

2.4. Direct Ink Writing Printing

The yielding and rapid self-recovery behavior of hydrogel networks are crucial rheological features necessary for extrusion applications, especially with 3D-printing techniques such as DIW. While linear block copolypeptides may undergo gelation via the formation of complex 2D assemblies, assembly is slow. In contrast, 3-arm star-shaped analogues are observed to assemble faster into 3D hydrogel networks with rapid reassociation of β-sheet domains leading to self-recovery after shear-based extrusion.[44] To simulate such an extrusion process, shear processing properties and recovery of samples with the highest (3-CP-PG) and lowest (3-CP-T) yield stresses were evaluated using cyclic oscillatory experiments, in which the strain amplitude was cycled in a step-wise fashion (**Figure 5**). Specifically, hydrogels were subjected to 0.1% and 100% strain for fixed periods of 100 s, allowing network stability at low strains and shear-yielding behavior at higher strains to be demonstrated. The storage modulus of 3-CP-PG decreased from 20 to 0.6 kPa, but quickly recovered back to its original value, signifying network recovery (Figure 5B). In contrast, 3-CP-T forms weaker networks (3 kPa) that rapidly decrease to 0.05 kPa and reform over similar strain cycles (Figure 5C). Because effective extrusion necessitates fast hydrogel yielding in the printer nozzle and shear-thinning during deposition onto the platform, rotational rheometry was used to better understand the non-Newtonian

properties of these materials (Figure 5D). Although 3-CP-PG forms a more viscous fluid at low shear compared to 3-CP-T, both materials flow similarly after yielding at high shear rates, simulating the printing extrusion process. Given these similarities in flow, the faster recovery and higher quiescent modulus of 3-CP-PG make it a better candidate for DIW compared to 3-CP-T.

To further demonstrate the impact of β-sheet structure on printability, 3-CP-PG and 3-CP-T were evaluated on a commercial DIW 3D-printer. Block copolypeptide hydrogels (20 wt%) were loaded into a 3 mL syringe (27-gauge nozzle), with filament size and print uniformity studied at various applied pressures during extrusion using Image J (**Figure 6**A). 3-CP-PG required higher applied pressures to extrude a stable filament, which directly correlates with the higher yield stress observed by rheometry. Both samples could form stable filaments with a width of 200 µm at their respective lowest extrudable pressures, although 3-CP-PG produced more consistent filaments with better shape fidelity. The larger variability in filament size for 3-CP-T is likely related to slower network recovery and lower yield/flow point.[55] While we have previously shown the ability of analogous hydrogels to print multilayered 3D structures, here the resolution of intricate two-layered patterns were studied.[38] In particular, the differences in filament uniformity is exacerbated when printing a two-layer complex lattice in the x–y plane that can be semi-quantified using printability (P_r) values (Equation (S2), Supporting Information).[14,55] The fast recovering, higher yield-stress 3-CP-PG gives a P_r value of 1.03 at 170 kPa, while the slower recovering and weaker 3-CP-T gives a P_r value of 1.2 at 40 kPa (Figure 6B and Figure S33, Supporting Information). In addition, 3-CP-PG hydrogels clearly show enhanced shape fidelity and better performance in 3D-printing. The modular nature of this 3-arm block copolypeptide platform provides good control over molecular design, architecture, hydrogel microstructure, rheological properties, and 3D-printability through synthetically tunable chemistry and eliminates the need for additives that are typically required to enhance the viscosity and shear-thinning properties of traditional, structurally fixed biopolymer inks.

3. Conclusion

In summary, we describe a robust strategy to create additive-free 3D-printable biomaterials based on β-sheet–driven hydrogelation of 3-arm star block copolypeptides that are readily synthesized using NCA ROP. The effects of changing spacer length and side-chain polarity on network properties were studied using valine, leucine, phenyl glycine, phenyl alanine, and tyrosine. All 3-arm block copolypeptides spontaneously form stable hydrogels with network structure and viscoelasticity determined by outer-block chemistry and degree of polymerization. This strategy provides access to different engineered properties, such as tailored thixotropy, yielding, and recovery. Significantly, these rheological differences were apparent during direct-ink writing, as the yielding and strain recovery trends correlate with filament uniformity and overall shape fidelity. In summary, our findings provide a basis to rationally design the 3D-printability and performance of sustainable, biocompatible polymers using amino-acid building blocks in tunable hydrogels.

Supporting Information

Supporting Information is available from the Wiley Online Library or from the author.

Acknowledgements

The research was sponsored by the U.S. Army Research Office and was accomplished under Cooperative Agreement W911NF-19-2-0026 for the Institute for Collaborative Biotechnologies. R.V.G. was partially supported and made use of shared facilities of the BioPACIFIC Materials Innovation Platform of the National Science Foundation under Award No. DMR-1933487. The research reported here made use of shared facilities of the UC Santa Barbara MRSEC (NSF DMR-2308708), a member of the Materials Research Facilities Network (www.mrfn.org). R.V.G. and E.A.M. were supported by the National Science Foundation Graduate Research Fellowship Program. N.S. acknowledges funding from the UC Santa Barbara MRSEC (NSF DMR-1720256, IRG-3).

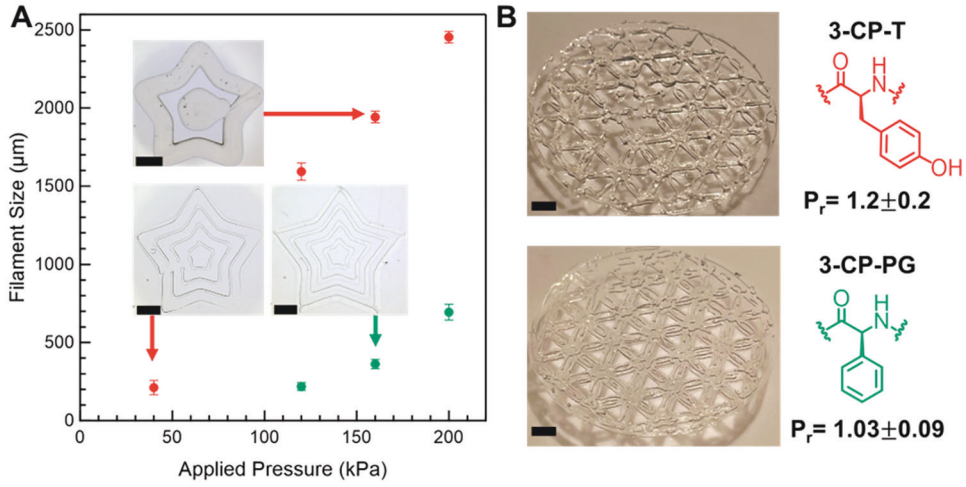

Figure 6. A) Filament width as a function of applied pressure and representative prints. B) 3-CP-T extruded at 40 kPa (top) and 3D-printed lattice of 3-CP-PG extruded at 170 kPa through a 27G needle (bottom) (Scale bars: 2 mm).

Conflict of Interest

The authors declare no conflict of interest.

Author Contributions

The manuscript was written by R.V.G., E.A.M., N.J.S., M.E.H., C.M.B., C.J.H., R.D.M., and J.R.A. Experiments were designed by R.V.G., E.A.M., N.J.S., J.M.U., C.J.H., R.D.M., and J.R.A., and performed by R.V.G., E.A.M., Y.O., and R.D.M. All the authors have given approval to the final version of the manuscript.

Data Availability Statement

The data that support the findings of this study are available from the corresponding author upon reasonable request.

Keywords

3D printing, direct-ink writing, hydrogels, polypeptides, writability

Received: April 3, 2023
Revised: May 30, 2023
Published online:

[1] K. Tian, J. Bae, S. E. Bakarich, C. Yang, R. D. Gately, G. M. Spinks, M. in het Panhuis, Z. Suo, J. J. Vlassak, *Adv. Mater.* **2017**, *29*, 1604827.
[2] E. Howard, M. Li, M. Kozma, J. Zhao, J. Bae, *Nanoscale* **2022**, *14*, 17887.
[3] S. M. Hull, L. G. Brunel, S. C. Heilshorn, *Adv. Mater.* **2022**, *34*, 2103691.
[4] C. Yu, J. Schimelman, P. Wang, K. L. Miller, X. Ma, S. You, J. Guan, B. Sun, W. Zhu, S. Chen, *Chem. Rev.* **2020**, *120*, 10695.
[5] A. P. Liu, E. A. Appel, P. D. Ashby, B. M. Baker, E. Franco, L. Gu, K. Haynes, N. S. Joshi, A. M. Kloxin, P. H. J. Kouwer, J. Mittal, L. Morsut, V. Noireaux, S. Parekh, R. Schulman, S. K. Y. Tang, M. T. Valentine, S. L. Vega, W. Weber, N. Stephanopoulos, O. Chaudhuri, *Nat. Mater.* **2022**, *21*, 390.
[6] S. Correa, A. K. Grosskopf, H. L. Hernandez, D. Chan, A. C. Yu, L. M. Stapleton, E. A. Appel, *Chem. Rev.* **2021**, *121*, 11385.
[7] K. Dubbin, Z. Dong, D. M. Park, J. Alvarado, J. Su, E. Wasson, C. Robertson, J. Jackson, A. Bose, M. L. Moya, Y. Jiao, W. F. Hynes, *Nano Lett.* **2021**, *21*, 1352.
[8] E. Sanchez-Rexach, P. T. Smith, A. Gomez-Lopez, M. Fernandez, A. L. Cortajarena, H. Sardon, A. Nelson, *ACS Appl. Mater. Interfaces* **2021**, *13*, 19193.
[9] P. T. Smith, G. Altin, S. C. Millik, B. Narupai, C. Sietz, J. O. Park, A. Nelson, *ACS Appl. Mater. Interfaces* **2022**, *14*, 21418.
[10] D. G. Karis, R. J. Ono, M. Zhang, A. Vora, D. Storti, M. A. Ganter, A. Nelson, *Polym. Chem.* **2017**, *8*, 4199.
[11] M. Tang, Z. Zhong, C. Ke, *Chem. Soc. Rev.* **2023**, *52*, 1614.
[12] U. N. Lee, J. H. Day, A. J. Haack, R. C. Bretherton, W. Lu, C. A. Deforest, A. B. Theberge, E. Berthier, *Lab Chip* **2020**, *20*, 525.
[13] M. Shahbazi, H. Jäger, *ACS Appl. Bio Mater.* **2021**, *4*, 325.
[14] L. Ouyang, R. Yao, Y. Zhao, W. Sun, *Biofabrication* **2016**, *8*, 035020.
[15] A. S. Gladman, E. A. Matsumoto, R. G. Nuzzo, L. Mahadevan, J. A. Lewis, *Nat. Mater.* **2016**, *15*, 413.
[16] T. Gao, G. J. Gillispie, J. S. Copus, A. P. R. Kumar, Y. -J. Seol, A. Atala, J. J. Yoo, S. J. Lee, *Biofabrication* **2018**, *10*, 034106.
[17] A. C. Yu, A. A. A. Smith, E. A. Appel, *Mol. Syst. Des. Eng.* **2020**, *5*, 401.
[18] M. T. Cook, P. Haddow, S. B. Kirton, W. J. Mcauley, *Adv. Funct. Mater.* **2021**, *31*, 2008123.
[19] A. R. Mazo, S. Allison-Logan, F. Karimi, N. J. A. Chan, W. Qiu, W. Duan, N. M. O'Brien-Simpson, G. G. Qiao, *Chem. Soc. Rev.* **2020**, *49*, 4737.
[20] H. He, M. Sofman, A. J. -S. Wang, C. C. Ahrens, W. Wang, L. G. Griffith, P. T. Hammond, *Biomacromolecules* **2020**, *21*, 566.
[21] S. H. Hiew, H. Mohanram, L. Ning, J. Guo, A. Sánchez-Ferrer, X. Shi, K. Pervushin, Y. Mu, R. Mezzenga, A. Miserez, *Adv. Sci.* **2019**, *6*, 1901173.
[22] Z. Song, H. Fu, R. Wang, L. A. Pacheco, X. Wang, Y. Lin, J. Cheng, *Chem. Soc. Rev.* **2018**, *47*, 7401.
[23] D. Huesmann, A. Birke, K. Klinker, S. Türk, H. J. Räder, M. Barz, *Macromolecules* **2014**, *47*, 928.
[24] M. T. Krejchi, E. D. T. Atkins, A. J. Waddon, M. J. Fournier, T. L. Mason, D. A. Tirrell, *Science* **1994**, *265*, 1427.
[25] S. Bera, S. Mondal, S. Rencus-Lazar, E. Gazit, *Acc. Chem. Res.* **2018**, *51*, 2187.
[26] N. J. Sinha, D. Wu, C. J. Kloxin, J. G. Saven, G. V. Jensen, D. J. Pochan, *Soft Matter* **2019**, *15*, 9858.
[27] A. M. Hilderbrand, E. M. Ford, C. Guo, J. D. Sloppy, A. M. Kloxin, *Biomater. Sci.* **2020**, *8*, 1256.
[28] A. P. Nowak, V. Breedveld, D. J. Pine, T. J. Deming, *J. Am. Chem. Soc.* **2003**, *125*, 15666.
[29] A. Jangizehi, M. Ahmadi, S. E. Seiffert, *Mater. Adv.* **2021**, *2*, 1425.
[30] A. C. Farsheed, A. J. Thomas, B. H. Pogostin, J. D. Hartgerink, *Adv. Mater.* **2023**, *35*, 2210378.
[31] R. D. Murphy, R. V. Garcia, A. Heise, C. J. Hawker, *Prog. Polym. Sci.* **2022**, *124*, 101487.
[32] R. Murphy, D. P. Walsh, C. A. Hamilton, S. A. Cryan, S.-A. Cryan, M. in het Panhuis, A. Heise, *Biomacromolecules* **2018**, *19*, 2691.
[33] M. Byrne, R. Murphy, A. Kapetanakis, J. Ramsey, S. A. Cryan, A. Heise, *Macromol. Rapid Commun.* **2015**, *36*, 1862.
[34] S. Zhang, D. J. Alvarez, M. V. Sofroniew, T. J. Deming, *Biomacromolecules* **2015**, *16*, 1331.
[35] M. A. Gonzalez, J. R. Simon, A. Ghoorchian, Z. Scholl, S. Lin, M. Rubinstein, P. Marszalek, A. Chilkoti, G. P. López, X. Zhao, *Adv. Mater.* **2017**, *29*, 1604743.
[36] N. J. Chan, S. Lentz, P. A. Gurr, T. Scheibel, G. G. Qiao, *Prog. Polym. Sci.* **2022**, *130*, 101557.
[37] A. C. G. Weiss, S. J. Shirbin, H. G. Kelly, Q. A. Besford, S. J. Kent, G. G. Qiao, *ACS Appl. Mater. Interfaces* **2021**, *13*, 33821.
[38] R. D. Murphy, R. V. Garcia, S. J. Oh, T. J. Wood, K. D. Jo, J. Read de Alaniz, E. Perkins, C. J. Hawker, *Adv. Mater.* **2023**, *35*, 2207542.
[39] C. C. Tang, S. H. Zhang, T. H. M. Phan, Y. C. Tseng, J. S. Jan, *Polymer* **2021**, *228*, 123891.
[40] Y. Sun, T. J. Deming, *ACS Macro Lett.* **2019**, *8*, 553.
[41] V. Breedveld, A. P. Nowak, J. Sato, T. J. Deming, D. J. Pine, *Macromolecules* **2004**, *37*, 3943.
[42] B. Wu, S. B. Hanay, S. D. Kimmins, S.-A. Cryan, D. H. Merino, A. Heise, *ACS Macro Lett.* **2022**, *11*, 323.
[43] Z. Y. Tian, Z. Zhang, S. Wang, H. Lu, *Nat. Commun.* **2021**, *12*, 5810.
[44] Y. Shen, S. Zhang, Y. Wan, W. Fu, Z. Li, *Soft Matter* **2015**, *11*, 2945.
[45] W. Zhao, Y. Gnanou, N. Hadjichristidis, *Chem. Commun.* **2015**, *51*, 3663.
[46] H. Yang, S. Yang, J. Kong, A. Dong, S. Yu, *Nat. Protoc.* **2015**, *10*, 382.
[47] V. M. Prabhu, E. J. Amis, D. P. Bossev, N. Rosov, *J. Chem. Phys.* **2004**, *121*, 4424.
[48] M. J. Solomon, P. T. Spicer, *Soft Matter* **2010**, *6*, 1391.
[49] P. M. De Molina, S. Lad, M. E. Helgeson, *Macromolecules* **2015**, *48*, 5402.

[50] S. Lin-Gibson, R. L. Jones, N. R. Washburn, F. Horkay, *Macromolecules* **2005**, *38*, 2897.
[51] N. Cohen, C. D. Eisenbach, *ACS Biomater. Sci. Eng.* **2020**, *6*, 1940.
[52] S. Lifson, C. Sander, *Nature* **1979**, *282*, 109.
[53] C. Yan, A. Altunbas, T. Yucel, R. P. Nagarkar, J. P. Schneider, D. J. Pochan, *Soft Matter* **2010**, *6*, 5143.
[54] C. Yan, D. J. Pochan, *Chem. Soc. Rev.* **2010**, *39*, 3528.
[55] A. Schwab, R. Levato, M. D'Este, S. Piluso, D. Eglin, J. Malda, *Chem. Rev.* **2020**, *120*, 11028.